ORIGINAL ARTICLE
Iran J Allergy Asthma Immunol
June 2025; 24(3):313-333.
DOI:10.18502/ijaai.v24i3.18682

A Novel Nanodrug Suppresses Lung Cancer Growth and Metastasis in C57BL/6 Mouse Model by Altering CD8$^+$ Cell Infiltration and Oxidative Stress

Sajjad Shekarchian[1], Marzieh Eghtedardoost[2], Hannaneh Golshahi[3], Helia Behrouzfar[4], Zahra Fakhroueian[5], and Roya Yaraee[1]

[1] Department of Immunology, Faculty of Medicine, Shahed University, Tehran, Iran
[2] Arena Best Diagnostics Lab Ltd., Tehran, Iran
[3] Nanobiotechnology Research Center, Avicenna Research Institute, ACECR, Tehran, Iran
[4] Faculty of Veterinary Medicine, Science and Research Branch of Islamic Azad University, Tehran, Iran
[5] School of Chemical Engineering-Nanomedicine, College of Engineering and IPE, University of Tehran, Tehran, Iran

Received: 6 October 2024; Received in revised form: 18 November 2024; Accepted: 24 November 2024

ABSTRACT

Lung cancer is a leading cause of cancer deaths worldwide and new therapeutic approaches are needed. This study investigates the efficacy of a new zinc oxide-based nanomedicine in a mouse model of heterotopic lung cancer.

C57BL/6 mouse model with Lewis lung carcinoma (LL2) cells was used. The mice were treated with different doses of nanodrug, cisplatin, or phosphate-buffered saline. Tumor growth, metastasis, markers for oxidative stress, and immune responses, in particular the infiltration of CD8$^+$ T cells, were examined.

The nanodrug significantly reduced tumor size, inhibited metastasis, and improved survival compared to the control group. Moreover, no significant toxic effect was observed in hematological, biochemical and histopathological analyses. Furthermore, the nanodrug altered the tumor microenvironment in favor of immune system activation by modulating the level of oxidative stress and increasing CD8$^+$ cell infiltration.

The results show that this new nanomedicine may be a candidate for an effective treatment for lung cancer.

Keywords: Animal model; Lung cancers; Nanomedicine; Nanoparticle; NSCLC; Zinc oxide

INTRODUCTION

In recent years, nanotechnology has emerged as an interesting field for the treatment of cancer.[1] Zinc oxide nanoparticles (ZnO NPs) have been extensively studied for their utility in cancer diagnosis, controlled drug release, and cancer therapy.[2] ZnO NPs have added value compared to other types of particles, namely high

Corresponding Authors: Zahra Fakhroueian, PhD;
School of Chemical Engineering-Nanomedicine, College of Engineering and IPE, University of Tehran, Tehran, Iran. Tel: (+98 21) 8208 4743, Fax: (+98 21) 8863 2976, Email: fakhroueian@ut.ac.ir.ac.ir

Roya Yaraee, PhD;
Department of Immunology, Faculty of Medicine, Shahed University, Tehran, Iran. Tel: (+98 21) 51212654, Fax: (+98 21) 51212602, Email: ryaraee@gmail.com

biocompatibility, negligible toxicity, and the ability to trigger, in particular, the formation of some reactive oxygen species ROS and the resulting induction of apoptosis.[2,3] These properties of ZnO NPs make them favorable candidates in the field of cancer treatment.[3] Some studies show that ZnO NPs can be used to combat various types of tumors, including breast, lung, and liver cancer.[2,4] Further research is required to obtain a complete overview of the effect of ZnO NPs in cancer treatment. Nevertheless, existing evidence suggests that ZnO NPs are a promising topic in the fight against cancer .[5-7]

Lung cancer is a very serious health condition whereby a person can experience great harm and in case of severe condition also death. The sheer fact that lung cancer is responsible for the highest death rate from this illness among both men and women is one of the reasons the disease is considered the top one.[8] Smoking is the main cause of lung cancer leading to about 85% of the cases in both men and women.[8] Lung cancer is usually diagnosed in the late stage of the disease when it is difficult to treat.[8] The diagnosis of lung cancer includes physical examination, medical history, X-ray, computed tomography (CT), magnetic resonance imaging (MRI), positron emission tomography (PET), sputum cytology, and biopsy.[9] The treatment includes operation, chemotherapy, and radiation therapy.[10] Lung cancer treatment may involve chemotherapy, which includes drugs like docetaxel, cisplatin, gemcitabine, nab-paclitaxel, paclitaxel, pemetrexed, and vinorelbine, and targeted therapies, such as erlotinib.[11,12] Surgical intervention for lung cancer includes medical procedures, such as lung lobectomy, lung wedge resection, lung resection, and pneumonectomy.[13-15] To establish the development of more effective modes of treatment and drugs for lung cancer, the use of further study is the next step.

The body's immune system is essential not only for defense but also for the development of a lung tumor.[16] Meanwhile, oxidative stress and cellular immunity, mainly $CD8^+$ T cells, are the major components for defense against lung cancer.[17-19] The term "oxidative stress" describes the breakdown of the equilibrium between the generation of ROS and the cells' ability to eliminate them. ROS can damage lipids, proteins, and DNA, and they are specifically aimed at cells. This could lead to mutation or cell death.[18] The immune system's defense against tumor cells is carried out by $CD8^+$ T cells, releasing cytotoxic molecules like granzyme B and perforin, which can injure and kill tumor cells.[20] studies have indicated that higher levels of $CD8^+$ T cells are associated with improved prognosis and lower mortality rates in lung cancer patients.[20] The connection between the increased levels of oxidative stress in the tumor microenvironment (TME) and the process of tumor growth and metastasis has been explored for the last few years.[18] However, when excessive oxidative stress occurs, it becomes a signal that exceeds the cell's detoxification capacity. This causes the process of both apoptosis and pyroptosis.[18] Therefore, targeting oxidative stress in tumor cells could be an effective strategy for treating lung cancer. The exact mechanism by which ZnO NPs affect oxidative stress and cellular immunity, particularly $CD8^+$ T cells, in lung cancer treatment is not fully understood. However, it has been suggested that ZnO NPs may increase oxidative stress in tumor cells, thereby enhancing apoptosis and pyroptosis.[21,22] Subsequently, they may reduce oxidative stress in the TME by increasing the activity of antioxidant enzymes and scavenging free radicals.[23] Additionally, ZnO NPs may increase cellular immunity by promoting cell death in cancer cells and reducing oxidative stress in the TME, thereby increasing the number of $CD8^+$ T cells and their cytotoxic activity against tumor cells.[24] Further research is necessary to fully elucidate the mechanisms underlying these processes. Therefore, ZnO NPs have great potential for use in the treatment of lung cancer by reducing oxidative stress in the TME and enhancing cellular immunity, especially that of $CD8^+$ T cells, whose role is crucial in the treatment of lung cancer. However, further research should be conducted to fully understand the mechanisms involved.

Previous in vitro investigations have been conducted on this nanodrug.[25] The current study aimed to investigate the impact of a novel surface-modified form of ZnO NPs on a heterotopic mouse model of lung cancer. This hypothesis suggests that the modifications made to this nanodrug will result in its sensitization and activation under metabolically active conditions, such as dividing cancer cells and cells experiencing pathological stress. This activation is supposed to enhance the generation of ROS inside the cancer cells and therefore give relative specificity to these surface-modified ZnO NPs for targeting the cancer cells. The present study evaluated the efficacy of the nanodrug and its toxicity, if any, in the heterotopic mouse model of lung cancer. Furthermore, this research assessed the factors participating in

oxidative stress and cellular immunity, after which a survival analysis was conducted for 30 days.

MATERIALS AND METHODS

Study Design

In this study, a total of 13 groups, each comprising five C57BL/6 mice aged 6–8 weeks old, were included. Following the successful implementation of the cancer model and its subsequent verification, 1 group was ethically sacrificed on day 0. The remaining 6 groups were administered PBS, cisplatin (cis-Diammineplatinum (II) dichloride, Sigma, Cat. No. P4394, St. Louis, MO, USA) at a dosage of 6 μg/kg,[26,27] and nanodrug at doses of 1.5, 3, 5, and 25 μg/kg via an oral feeding tube and diet every other day. nanodrug doses (1.5–25 μg/kg) were chosen based on prior research and preliminary tests in C57BL/6 mice. This range balanced efficacy and safety, avoiding low-dose inefficiency and high-dose toxicity.[5,6] These groups were then observed for 15 days. Additionally, another 6 groups were administered the same substances and kept under observation for a period of 30 days for survival analysis. At the end of each observation period, the mice were humanely euthanized and analyzed in accordance with relevant ethical principles.

Nanoparticle Synthesis and Characterization

According to the basis and mechanism of the synthesis of this special new nanodrug (oxidation-reduction reaction), which was formulated for the first time, strong oxidizing and reducing nanocomposites have been used in nanoformulations.[10] Nano oxidizer contains alcoholic function and reductant has carboxylic material. The synthesis methods are sol-gel, coprecipitation, and wet chemical methods. One of its important oxidizing agents is ZnO NPs, whose surface is modified with a healthy hydrophilic substance and was synthesized by the sol-gel method through the alkaline hydrolysis of zinc acetate dihydrate salt. To maintain the stability of the organic nanocomposites, polyethylene glycol polymer with a molecular mass of 4000 to 6000 was used in distilled water as a nanofluid stabilizer. To prepare the final nanoformulation of this nanodrug, we used the wetting agent ethoxylated, pharmaceutical green solvents, biodegradable surfactant based on a natural compound, and sorbitan hydrophilic emulsifier at an optimal pH of 7 to 8. In this study, none of the consumables were toxic or dangerous. Nanodrug is completely eco-friendly and complies with the FDA health regulations. One of the advantages of this synthesis is that, during the reflux of the product for a few hours, the color of the solution suddenly changes from gray to black, which is a key sign of the completion of the formulation. This means that the main ingredients in the product have been able to use dispersants, emulsifiers, and wetting agents in aqueous solvents through the synergistic effect created between themselves, which are combined to produce a homogeneous product with high activity. Creating this class of nanoformulations is not an easy task. This requires special precision, skill, and patience. The nanoparticle characterization was assessed using parameters including ultraviolet-visible (UV-vis) (Model: Shimadzu-UV-2550), FTIR (Model: PerkinElmer-Spectrum Two), FESEM (Model: ZEISS-Sigma VP), XRD (Model: Panalytical-X' Pert Pro), and DLS-Zeta (Model: HORIBA-nanoPartica SZ-100V2 Series).

LL2 Cell Culture

To induce the model in mice, the initial step involved the preparation of the LL2 cell line procured from the Pasteur Institute of Iran. The cells were then cultured and injected into mice. The cells were cultivated in an incubator with 5% CO_2 and 92% humidity, using Dulbecco's Modified Eagle Medium (DMEM) culture (Gibco, Cat. No. 11-965-092, Seoul, Korea) supplemented with 10% FBS (DNA biotech, Cat. No. DB9723-100 ml, I.R. Iran), and penicillin-streptomycin (Gibco, Cat. No. 15140, Seoul, Korea).

Animal Model and Treatment

Five pilot mice were injected subcutaneously into the flank region with 5×10^5 LL2 cells. Following a 15-day observation period, tumor growth was evident in the flank region, and by day 50, the tumors in 3 mice had reached the desired size for transplantation. Three days prior to transplantation, recipient mice were immunosuppressed with cyclosporine A (Thermo Scientific, Cat. No. 457970010, Waltham, MA, USA) at a dosage of 12.5 mg/kg.[28] Subsequently, 3 tumor fragments, measuring approximately 2–3 mm, were excised from the pilot mice and implanted subcutaneously into the flank region of anesthetized recipient mice. After an additional 15 days, tumor formation was clinically confirmed in 75 mice, which were designated for further investigation.

Published by Tehran University of Medical Sciences (http://ijaai.tums.ac.ir)

Blood Collection and Tissue Sampling

Upon completion of the designated study period for each cohort of mice, animals were humanely euthanized in accordance with established ethical guidelines. Subsequently, cancerous and other vital organ samples were collected. Finally, the slides of tissues were stained with hematoxylin and eosin (H&E) (Carlroth, Cat. No. 9194.2, Baden-Wurttemberg, Germany) to facilitate subsequent histopathological examinations. The slides were observed by a veterinary pathologist (Dr. H. Golshahi) via direct optical microscopy (Olympus BX53) at 20× and 40× magnifications. Whole blood and serum samples were obtained following the sacrifice procedure. The serum levels of alanine transaminase (ALT), aspartate transferase (AST), alkaline phosphatase (ALP), urea, and creatinine were assayed using Biorex Fars Biochemistry Analyte Kits, and blood cells and hematological factors were counted using a veterinary cell counter (Exigo-Boule Medical).

Immunohistochemical Staining

To examine the infiltration of $CD8^+$ cells within the tumor microenvironment, immunohistochemistry was performed on tissue samples procured from the tumor site. The presence of cancer in these tissue samples was confirmed by a veterinary pathologist, and the slides were prepared accordingly. Additional tissue slides from the same samples were collected for the immunohistochemical assessment of CD8 markers. Immunohistochemistry was performed using standard methods. The anti-mouse CD8 primary antibody (Abcam, Cat. No. ab217344, Cambridge, UK) was diluted in 0.1% phosphate buffered saline (PBS)-bovine serum albumin (BSA). Subsequently, the slides were exposed to a secondary detection system (Abcam, Cat. No. ab64256, Cambridge, UK). The prepared slides were then mounted and imaged under a microscope.

Assessment of Oxidative Stress

Oxidative stress was assessed using superoxide dismutases (SOD) and malondialdehyde (MDA) markers. A sample weighing 0.25 grams was extracted from the frozen tissue and homogenized in 1 mL radioimmunoprecipitation assay buffer (RIPA) buffer solution. The homogenized tissues were then incubated at room temperature for 5 minutes, after which they were subjected to centrifugation (13000 rpm, 4°C, 20 minutes). The supernatant was isolated and transferred to a fresh microtube for further experiments. The protein concentration in each tissue was determined using a the bicinchoninic acid (BCA) Protein Assay Kit (Kiazist Company, Hamadan, Iran). The evaluation of SOD activity was performed using a ZellBio SOD Kit (CAT No. ZX-44108 -96, Germany), according to the manufacturer's protocol provided with the kit. MDA was evaluated using a ZellBio MDA Kit (CAT No. ZX-44116 -96, Germany), according to the manufacturer's protocol. Finally, the plates were read using a HiPerion $MPR4^{++}$ microplate reader.

Data Analysis Methods

Statistical analysis of the data pertaining to each experiment was conducted using GraphPad Prism software version 9.5.1. The analytical approach employed included descriptive statistics, including measures such as the mean and standard deviation, in addition to inferential statistics used to compare various groups. The statistical tests employed for general comparisons included ordinary one-way analysis of variance (ANOVA) and two-way repeated-measures ANOVA. Furthermore, the normality of the data was assessed using the Shapiro-Wilk test, and homoscedasticity or heteroscedasticity within groups was evaluated using the Levene test. Additionally, Grubbs' test was employed to confirm outlier data, and post hoc analysis after ANOVA was performed using the Tukey HSD (honestly significant difference) test.

RESULTS

The Nanoparticles with Desirable Properties and Modifications Were Successfully Synthesized for Use as Nanodrug

Nanoparticle characterization involves a variety of techniques to understand the properties and behaviors of nanoparticles. Figure 1 presents data from different characterization techniques, such as dynamic light scattering (DLS), zeta potential analysis, field emission scanning electron microscopy (FESEM), fourier transform infrared spectroscopy (FTIR), and X-ray Diffraction (XRD). Each method provides unique insights into nanoparticle size, stability, morphology, chemical composition, and crystallinity.

Dynamic Light Scattering Analysis of Nanoparticles

The DLS analysis of the nanoparticles reveals an average particle size of approximately 458.9 nm, with a mode of 426.3 nm and a Z-average of 947.0 nm (Figure

1E). A polydispersity index of 0.626 indicates moderate heterogeneity in the size distribution. The autocorrelation function and residual plots support the reliability of size measurements.[29,30] These characteristics are crucial for understanding the behavior of nanoparticles in biological systems, where size and distribution can significantly impact cellular uptake, biodistribution, and therapeutic efficacy.

Zeta Potential Analysis of Nanoparticles

The zeta potential (ζ) value of −7.8 mV indicates that the average charge of various NPs in the formulation is negative. Zeta potential is a key indicator of colloidal stability; NPs with zeta potential values between −30 mV and +30 mV are generally considered stable due to sufficient electrostatic repulsion preventing aggregation (Figure 1B). In this case, the negative charge suggests that the nanodrug formulation is likely to remain stable in suspension, reducing the risk of aggregation and ensuring a uniform distribution in biological environments.[31,32] A negative zeta potential indicates that the NPs have suitable adsorption on the positive charge of tumors and can diffuse into the cell membrane and produce chemical reactions with them.

Field Emission Scanning Electron Microscopy Analysis

The nanodrug under investigation was characterized using FESEM to elucidate its morphological features. The FESEM images shown in Figure 1C provide critical insights into the surface topography and structural attributes of the synthesized nanoparticles. FESEM micrographs revealed the presence of nanostructures with distinct morphologies. At a magnification of 10000× (left image), the nanoparticles exhibited a heterogeneous surface with clusters of particles varying in shape and size. These clusters appear to be aggregated, forming larger assemblies that are indicative of the inherent propensity of the material to agglomerate under certain conditions. The surface texture was uneven, suggesting possible variations in the particle formation process or the presence of multiple phases within the sample. At a higher magnification of 50000× (right image), more detailed structural characteristics were discerned. The zoomed-in view allows for a closer examination of individual nanoparticles and their respective dimensions. The particles exhibited a predominantly spherical to irregular morphology, with notable variations in their diameters. Quantitative analysis of the FESEM images indicated a broad size distribution of nanoparticles. Measurements annotated in the right image reveal nanoparticle sizes ranging from approximately 17.86 nm to 66.99 nm. This size distribution is critical for understanding the potential biomedical applications of the nanodrug, as particle size can significantly influence cellular uptake, biodistribution, and overall therapeutic efficacy. FESEM images with larger magnifications show the surface morphology and structure of their NPs in nanofluid. In the observed images of the surface morphology of this nanodrug, many small spherical nanoparticles as well as many stretched and extended NPs can be seen among the multitude of reagents used in nanofluid formulation. On the other hand, this characterization provides valuable data that can be correlated with the functional performance of the nanodrug.

X-Ray Diffraction Analysis of Nanoparticles

The XRD pattern presented in Figure 1D shows the diffraction peaks obtained from the nanoparticle sample. The X-axis represents the diffraction angle (2θ) in degrees, while the Y-axis denotes the intensity (counts) of the diffracted X-rays. The peaks in the XRD pattern correspond to the planes of atoms in the crystalline structure of the nanoparticles. The presence of distinct diffraction peaks at characteristic 2θ values confirms the presence of crystalline phases in the nanoparticles. The prominent peaks are observed at approximately 10°, 20°, 30°, 40°, 50°, 60°, and 70° 2θ positions. These peaks correspond to the Bragg reflections from specific crystallographic planes. Each peak can be indexed to a specific crystallographic plane using standard reference databases such as the Joint Committee on Powder Diffraction Standards (JCPDS) or the International Centre for Diffraction Data (ICDD). The presence of multiple diffraction peaks indicates that the nanoparticle sample is composed of multiple crystalline phases. By comparing the 2θ positions of the observed peaks with standard diffraction patterns, the specific phases present in the sample can be identified. The wide peak observed in the lower 2θ range (around 10° to 30°) suggests the presence of an amorphous phase in the nanoparticles sample (2θ=20.62°). Amorphous materials lack long-range order, resulting in broad, diffuse scattering instead of sharp diffraction peaks. The XRD diagram for the crystalized pure ZnO NPs powder with Cu–Kα radiation (λ=0.15406 nm) demonstrated that all of the diffraction peaks can be indexed as a typical hexagonal phase of

Published by Tehran University of Medical Sciences (http://ijaai.tums.ac.ir)

ZnO NPs including space group p63 mc, and showed Wurtzite structure with hexagonal phase according to lattice constant of a=b=3.249 Å and c=5.206 Å with JCPDS Card No. 36-1451. On the other hand, XRD analysis of the nanoparticle samples reveals a complex structure comprising both crystalline and amorphous phases. Short sharp peaks are also seen at 32 to 37 degrees. Very broad peaks represent very fine amorphous NPs and short sharp peaks represent crystallized other nanocomposites into the nanofluid. Usually, the average size of NPs can be calculated using the Debye Scherrer equation using the peak with 100% intensity. The crystalline structure of NPs is obtained by comparing JCPDS standard cards.[31]

Fourier Transform Infrared (FTIR) Spectroscopy Analysis of Nanoparticles

The FTIR spectrum provided in Figure 1E illustrates the transmission (%T) of infrared radiation through the nanoparticle samples across a wavenumber range of 4000 to 400 cm^{-1}. The X-axis represents the wavenumber (cm^{-1}), indicating the frequency of the infrared radiation, while the Y-axis shows the percentage of transmission (%T), with lower values indicating higher absorption. A broad absorption band is observed around 3432.85 cm^{-1}, which is characteristic of O-H stretching vibrations. This indicates the presence of hydroxyl groups in the nano-oxidant and solvent. Additionally, a sharp peak at 3774.82 cm^{-1} may also correspond to free O-H stretching vibrations, suggesting isolated hydroxyl groups. The peaks at 2919.87 cm^{-1} and 2851.68 cm^{-1} are indicative of C-H stretching vibrations from aliphatic hydrocarbons, suggesting the presence of alkyl groups in the nanofluid formulation. A significant peak at 1736.23 cm^{-1} is attributed to C=O stretching vibrations, which are characteristic of carbonyl functional groups such as ketones, aldehydes, carboxylic acids, or esters. The region around 1600–1500 cm^{-1} exhibits multiple peaks, with prominent bands at 1598.49 cm^{-1}, 1511.35 cm^{-1}, and 1463.19 cm^{-1}, corresponding to -C=C- stretching vibrations in aromatic rings and linear -C=C- chains. The region below 1000 cm^{-1} shows several peaks, such as 1107.57 cm^{-1}, 944.19 cm^{-1}, 837.15 cm^{-1}, and 546.47 cm^{-1}, which can be attributed to out-of-plane deformations of C-H bonds in aromatic rings, bending vibrations of C-H bonds, and other nanocomposites in this nanofluid and corresponds to the hexagonal wurtzite structure of Zn-O at the frequency of 546.47 cm.[1,31,3]

UV-Visible Spectroscopy Analysis of Nanoparticles

The UV-Vis spectra of 2 nanoparticle samples at different dilutions (1:50 and 1:250) are presented in Figure 1F. The X-axis represents the wavelength (nm), while the Y-axis indicates the absorbance. A measure of the amount of light absorbed by the sample. The spectrum of the nanoparticles at a 1:50 dilution shows a prominent absorption peak in the UV region, with a maximum absorbance around 2.5 at approximately 210 nm. This peak is likely due to π-π^* transitions of conjugated systems within the nanodrug. A secondary absorption feature appears around 280 nm, with significantly lower absorbance compared to the primary peak. This secondary feature may indicate the presence of additional chromophores or different electronic transitions. Beyond 300 nm, the absorbance rapidly decreases, with minimal absorption observed in the visible region (400–800 nm). This suggests the nanoparticles do not possess significant visible chromophores and are primarily characterized by their UV absorption properties. The UV-Vis spectrum of the nanoparticles at a 1:250 dilution exhibits a similar absorption profile to the 1:50 dilution sample but with lower absorbance values due to the higher dilution factor. The primary absorption peak around 210 nm shows a maximum absorbance of approximately 1.1, indicating that the concentration of the nanoparticles significantly influences the intensity of this peak. The secondary absorption feature around 280 nm is also present but with reduced intensity compared to the 1:50 dilution. Blue fluorescence emissions (blue shift) can be found because of many unique trapping states, electron-hole pairs, crystal defects, high-superficial surface energy, reactive sites due to smart surface modification and specific structural characteristics and physicochemical properties for ZnO NPs and various Nano-oxidizing and nano-reducing agent nanocomposites in this healthy nanodrug. Which shows the strong potential applications in biological fluorescent labels.[25] In addition, the UV-Vis emission peaks could show very fine particle sizes in nanofluid formulation containing high band gaps (the gap between the electron transfer from conduction and valance bands in semiconductor fine NPs), and various nano structural defects (oxygen vacancies and zinc-oxygen interstitials). Basically, according to the theory of quantum physics or (quantum confinement), as long as NPs absorb UV-Vis light at short wavelengths, they must be small (size-dependent emission). So, by having UV-Vis curves,

Published by Tehran University of Medical Sciences (http://ijaai.tums.ac.ir)

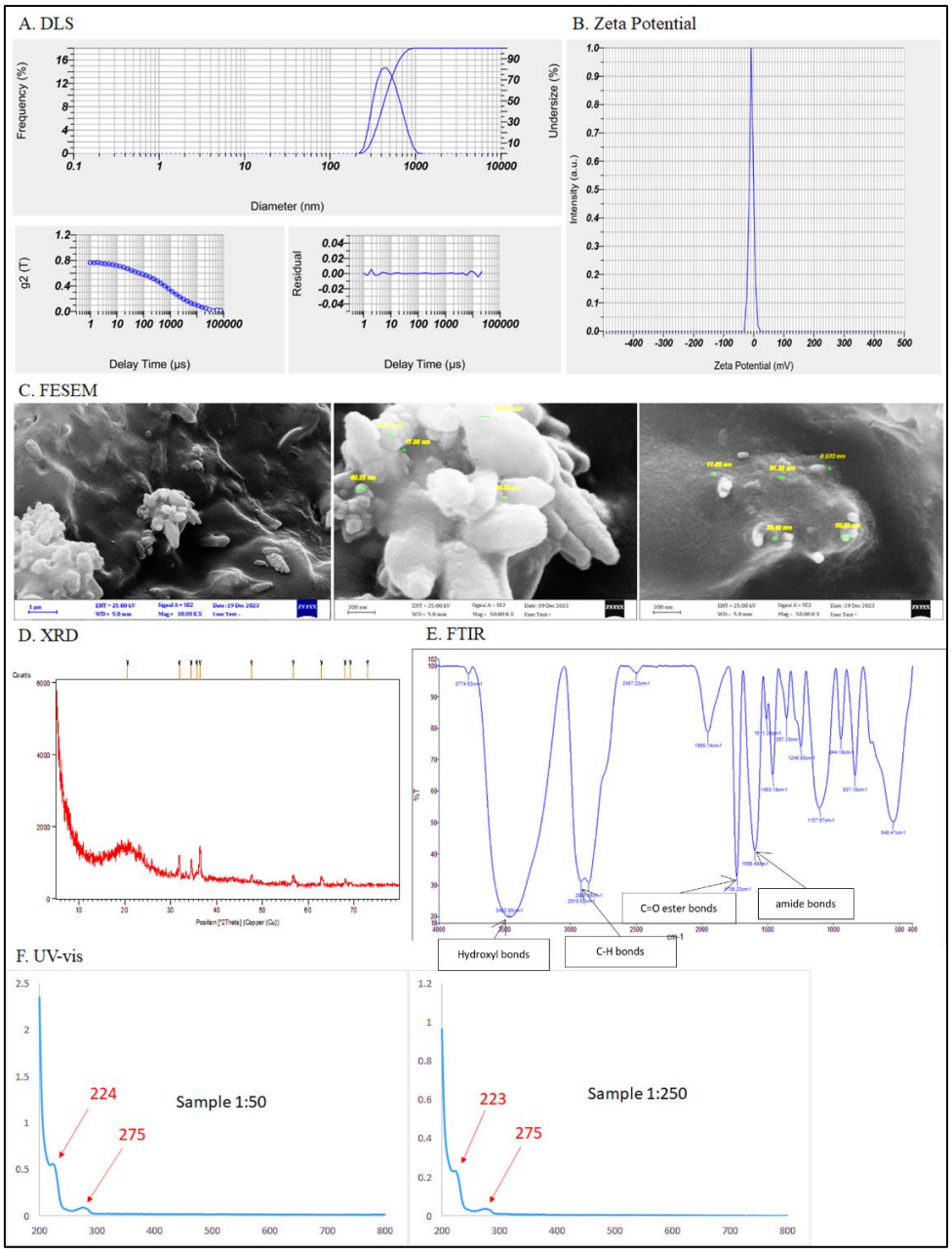

Figure 1. Characterization of Nanoparticle. This figure showcases the data from various characterization techniques used to evaluate the synthesized nanomedicine, demonstrating desirable characteristics and modifications suitable for nanodrug applications. A. Reveals an average particle size of approximately 458.9 nm with a polydispersity index of 0.626, indicating moderate size distribution heterogeneity. B. Shows a mean zeta potential of -7.8 mV, suggesting colloidal stability with a slightly negative surface charge, essential for preventing nanoparticle aggregation. C. Provides detailed images of the nanomedicine's surface morphology and particle size distribution, revealing nanoparticles ranging from 17.86 nm to 66.99 nm. D. Indicates the crystalline structure of the nanomedicine with distinct diffraction peaks, suggesting a complex structure comprising both crystalline and amorphous phases. E. Identifies specific functional groups such as hydroxyl, carbonyl, alkyl, and aromatic groups, offering insights into the chemical composition and potential interactions. F. Demonstrates the electronic structure and concentration-dependent behavior of the nanomedicine, with strong absorption in the ultraviolet (UV) range indicating the presence of conjugated systems or aromatic rings.

the size of NPs can be known. Therefore, the effective direct high band gap energy of special NPs increases with decreasing the mean particle size, which means that the absorption edges spectrum blue-shifts with decreasing particle size (Brus' model).[31,33]

The New Formulation of Nanodrug Exhibit a Satisfactory Effectiveness in Suppressing the Proliferation and Metastasis of Cancer Cells.

Thirteen cohorts of C57bl/6 mice were evaluated in the study on the timeline, as shown in Figure 2.1. One cohort of mice was sacrificed for the first time on day 1 of the study (OD). Subsequently, 6 additional cohorts of mice were sacrificed after 15 days, with 1 cohort treated with PBS, 1 with cisplatin, and 4 with nanodrug at doses of 1.5, 3, 5, and 25 μg/kg, respectively. An additional 6 cohorts underwent 30-day survival analysis and received the same treatments as mentioned above for the 15-day cohorts. At the end of each study period, the cancer tissues were collected and prepared for histopathological examinations, as shown in Figure 2.2. The existence of the tumor was confirmed in all mice examined by a veterinary pathologist (Figure 2.2 A-N).

The size of the tumor, serving as a measure of the proliferation of cancer cells, assumes a crucial role in evaluation of the efficacy of anticancer agents.[34] Moreover, in the event that anticancer agents possess the capacity to reduce the tumor's ability to metastasize, they are acknowledged as efficacious anticancer agents, thus rendering them a promising candidate for therapeutic applications.[35] This study examined the relationship between the size of tumors and the efficacy of nanodrugs against lung cancer cells within a mouse model over a 15-day period (Figure 2.3). The findings indicated that the cohorts administered with nanodrug and cisplatin exhibited reduced tumor sizes in comparison to those receiving PBS ($p<0.0002$). Notably, no disparity in tumor size was observed between the mice receiving nanodrug and cisplatin. Another factor that was assessed was the examination of metastasis in distant organs by the expert pathologist (Figure 3). As per the pathology report, on the initial day of the investigation, no instances of metastasis were observed in the mice that were sacrificed. Only 1 instance of metastasis was detected in the liver among the mice treated with nanodrug. For the mice treated with cisplatin, metastasis to the liver was observed in multiple instances, which was noteworthy. In the case of mice treated with PBS, in addition to severe liver metastasis, metastasis in other organs was also observed.

Survival analysis holds significant importance in the field of anticancer drugs as it provides a means to assess the effectiveness of a new drug candidate. In this study, survival analysis was conducted on 6 cohorts of mice, which were considered as previous cohorts. The distinguishing factor among these cohorts was that the mice were observed for a period of 30 days, during which their time of death was recorded and subjected to statistical analysis. The results obtained from this study, as depicted in Figure 2.4, revealed a notable increase in survival rates for mice treated with nanodrug and cisplatin, in comparison to those receiving PBS ($p<0.0001$).

The Nanodrug Demonstrated No Toxic Effects in Mice with Lung Cancer Model.

The evaluation of toxicity holds significant importance in the detection and determination of possible detrimental impacts caused by various chemical substances.[36] Given that no in vivo toxicological assessments have been conducted thus far regarding this nanodrug, subsequent to the sacrifice of the mice, not only were the cancerous tissues collected, but also the vital organs of the mice were procured and subjected to pathological, hematological, and biochemical study. These evaluations were augmented by weight measurement and clinical observations of the mice throughout the duration of the study, thereby affording us a more comprehensive perspective.

The findings of the hematological assessments are presented in Figure 3 A–D. The results indicated that the number of red blood cells (RBC) in cancerous mice did not exhibit a significant alteration across all cohorts. However, cohorts that received cisplatin and those that were administered with 1.5 and 3 μg/kg of nanodrugs showed a tendency towards restoring RBC levels to those observed in healthy mice.[37] Similarly, in terms of hematocrit and hemoglobin levels, the cohorts that received cisplatin and those that were treated with 1.5 and 3 μg/kg of nanodrug exhibited a significant tendency towards returning to normal levels, which differed from the other cohorts. With respect to blood platelets, while the mice receiving varying doses of nanodrug showed a significant increase in their blood platelet levels compared to the PBS group, it remained far from the normal level. Conversely, the blood platelets of mice

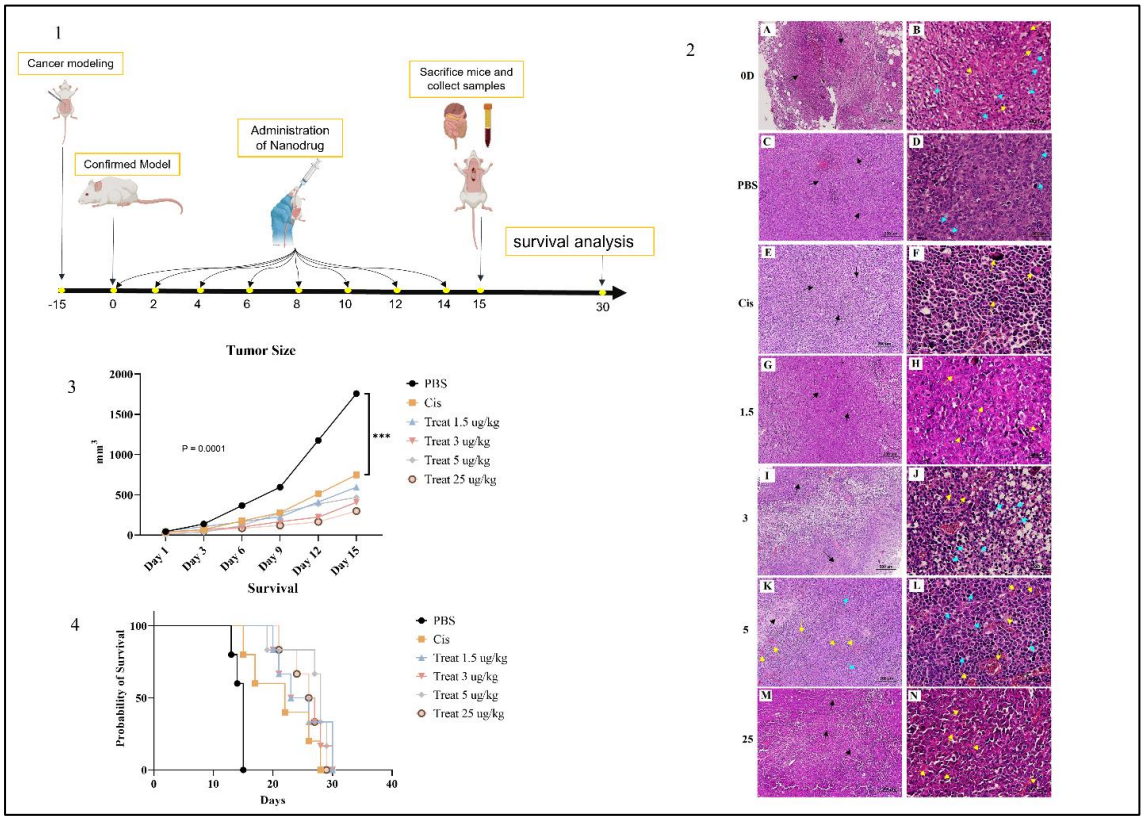

Figure 2. I. The timeline of the study. II. A. The tumor mass was composed of neoplastic cells arranged in a solid pattern surrounded by a fibrillar collagenous stroma (black arrow). B. Higher magnification of the previous slide, the neoplastic cells showed round features (blue arrow), also note the infiltration of neutrophils (yellow arrow) in the stroma. C. The tumor shows a solid growth pattern (black arrow). D. Higher magnification of the previous slide, note the mitotic figures (blue arrow). E. Tumor tissue consisted of sheaths of ovoid to round cells with poorly defined cytoplasm (black arrow). F. Higher magnification of the previous slide, note the bizarre cells (yellow arrow) within the tumor. G. Note the proliferation of the neoplastic cells (black arrow) arranged in a solid pattern surrounded by a fine fibrillar collagenous stroma. H. Higher magnification of previous slide, the tumor cells showed large vesicular nuclei and single prominent nucleoli (yellow arrow). I. The neoplastic cells revealed a solid pattern (black arrow). J. Higher magnification of previous slide: the nuclei of tumor cells were large and hyperchromatic (yellow arrow), also note the infiltration of inflammatory cells (blue arrow). K. Tumor tissue consisted of sheaths of ovoid to round cells with poorly defined cytoplasm (blue arrow). Also, note the angiogenesis (yellow arrow) and foci of necrosis (black arrow) within the tumor. L. Higher magnification of the previous slide, note to neoplastic cells (blue arrow) and noticeable angiogenesis (yellow arrow). M. The neoplastic cells with solid pattern (black arrow). N. Higher magnification of the previous slide, Infiltration of ovoid to round neoplastic cells with large vesicular nuclei and multiple prominent nucleoli (yellow arrow). (H and Scale bars A, C, E, G, I, K, M, 200 µm; B, D, F, H, J, L, 50 µm). III. During a 15-day period, the variations in tumor size among mice assigned to 15 distinct groups were observed and subjected to analysis. It was noted that the mice in the phosphate-buffered saline (PBS) group displayed a substantial increase in tumor growth compared to the other groups. Conversely, mice receiving the nanodrug and cisplatin exhibited a comparatively slower tumor growth rate. To assess the statistical significance of these findings, a two-way repeated measures analysis of variance (ANOVA) was performed. The outcomes revealed significant variance among the groups (p=0.0002), indicating that the type of drug administered had an impact on tumor growth. Furthermore, a significant disparity was observed over time (p=0.0001). IV. The Kaplan-Meier method was utilized to assess the survival outcomes of mice in the 30 groups. The results indicated a higher rate of mortality in mice treated with the PBS compared to the other group. Intriguingly, 2 mice from the nanodrug group survived without any significant clinical issues until day 30. To compare the survival outcomes across the groups, statistical analyses including the log-rank survival analysis (Mantel-Cox) test and the log-rank test for trend were performed (p<0.0001).

treated with cisplatin returned to normal levels.

The results of the biochemical tests are shown in Figure 3E–I. Creatinine and urea nitrogen are very important indicators of kidney function.[38] The results showed that there were no significant changes in these parameters in all groups except the cisplatin-treated group. However, after cisplatin treatment, the mice showed an affected increase in creatinine and urea nitrogen levels, which could be due to the progressive kidney damage that cisplatin caused (Figure 3). Liver function tests mainly monitor parameters such as ALT, AST, and ALP for liver health.[39] These parameters can be used to detect damage to the liver.[39] This study found that all three parameters were significantly higher in the mice treated with PBS. Furthermore, the cisplatin-treated mice tended to have increased levels of all 3 parameters compared to the nanodrug-treated group, where the trend in AST was statistically significant. The significant increase in ALT, AST and ALP in mice receiving PBS might be related to the severe liver metastasis of these mice. Furthermore, an increase in these 3 parameters in mice receiving cisplatin may indicate lesser forms of liver metastasis observed in these mice.

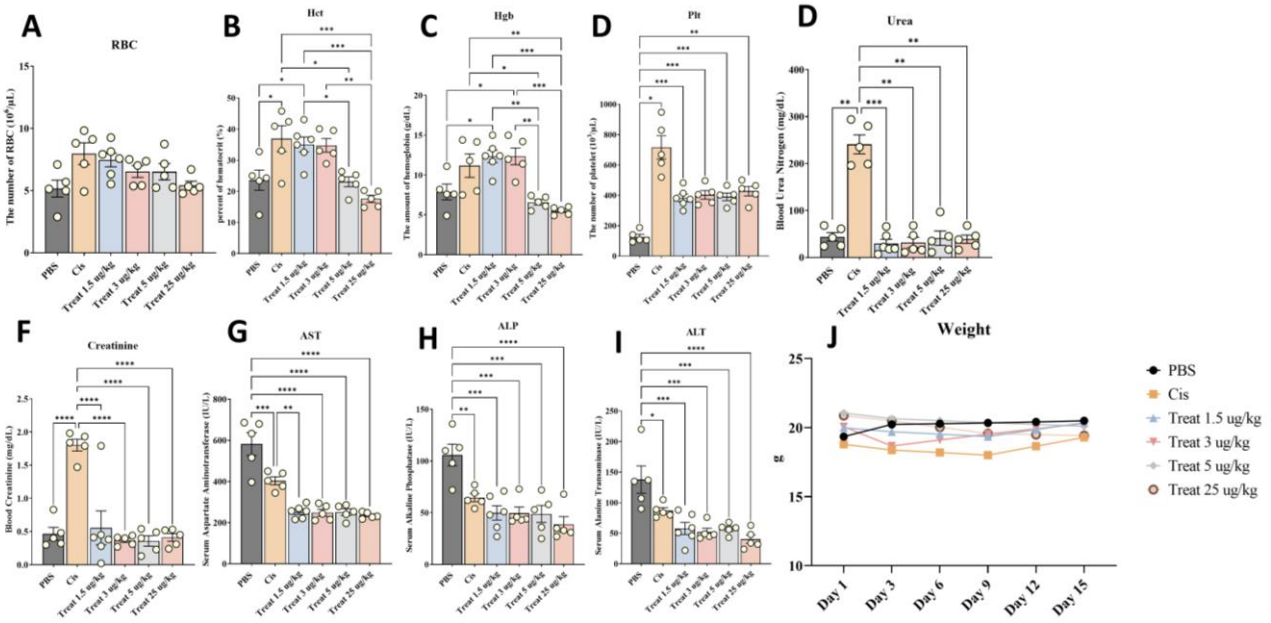

Figure 3. Evaluation of the toxicological effects of nanodrugs in vivo. The results show that the administration of cisplatin and certain doses of nanodrug had a positive impact on restoring red blood cells (RBC) (A), hematocrit (Hct) (B), and hemoglobin (Hgb) levels (C) in cancerous mice. However, the blood platelet levels (D) in mice treated with nanodrug remained significantly below normal, while those treated with cisplatin returned to normal levels. The evaluation of creatinine (f) and urea nitrogen levels (e) indicated significant elevation in mice treated with cisplatin, suggesting potential renal damage. Liver function tests revealed elevated levels of alanine transaminase *(*ALT) (g), aspartate transferase *(*AST) (h), and alkaline phosphatase *(*ALP) (i) in mice administered with PBS, as well as in mice treated with cisplatin, indicating potential liver damage. Statistical significance was determined by one-way analysis of variance (ANOVA) and Dunnett's posthoc test. ns: not significant, * $p<0.05$, ** $p<0.01$, *** $p<0.001$ and **** $p<0.0001$.

To gain deeper insight into the effect of the nanodrug on the vital organs of mice, a veterinary pathologist conducted histopathological examinations of these organs (Figure 4). The results of histopathological examination showed that mice treated with cisplatin experienced progressive tissue destruction of their kidney tissue. In contrast, no cases of tissue damage in vital organs due to nanodrug toxicity have been reported.

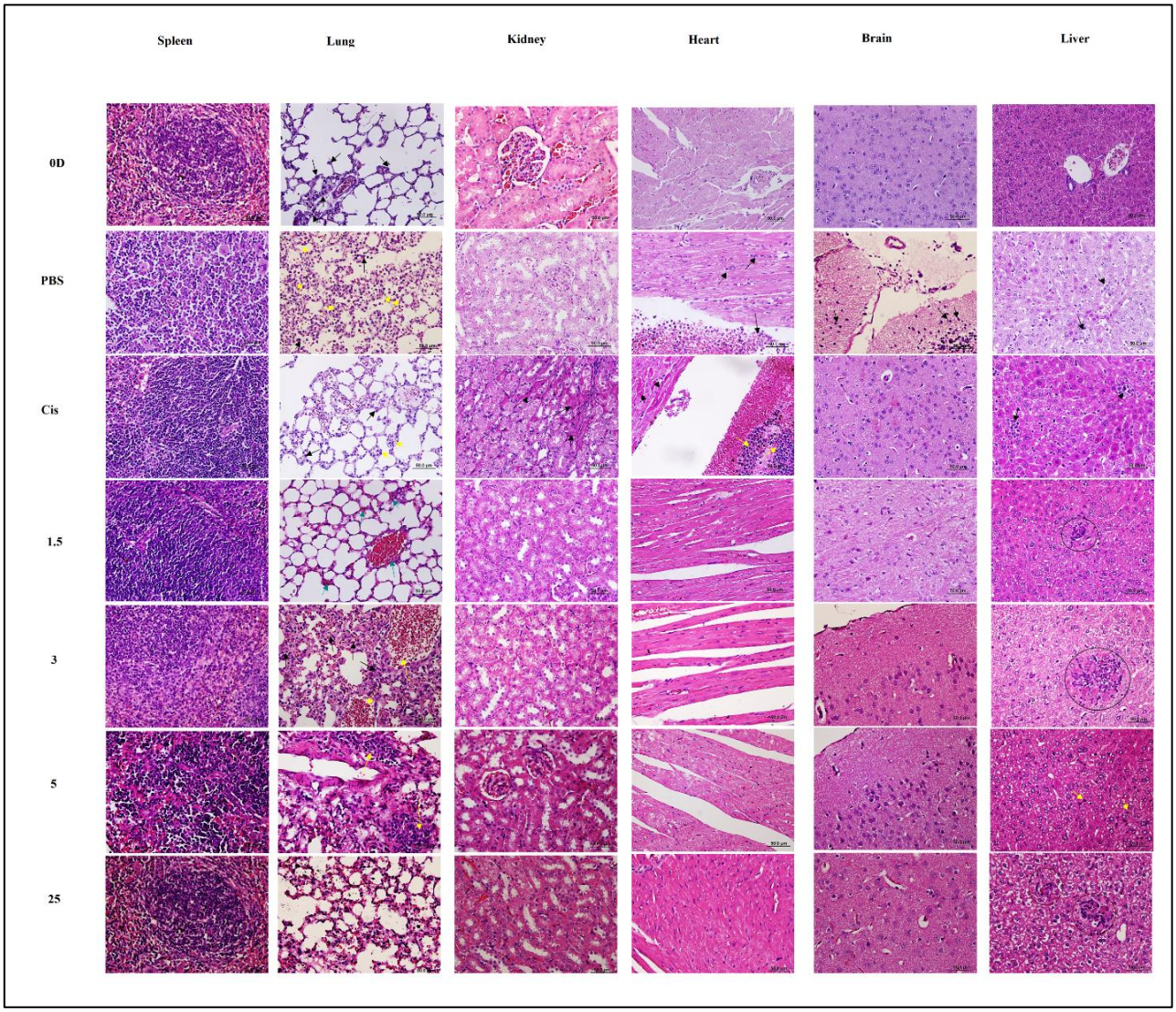

Figure 4. Microscopic evaluation of various organs across different groups. Spleen: 0D: Normal histology, PBS: Normal histology, Cis: Normal histology, 1.5: Normal histology, 3: Normal histology, 5: Normal histology, 25: Normal histology. Lung: 0D: Normal histology, PBS: Infiltration of neutrophils in the parenchyma (yellow arrow) and the presence of a limited number of tumor cells in the pulmonary tissue (black arrow), Cis: Infiltration of inflammatory cells (yellow arrow) and individual tumor cells in the pulmonary parenchyma (black arrow), 1.5: Mild hyperemia noted (green arrow), 3: Thickening of alveolar septa due to accumulation of inflammatory cells (black arrow) and hyperemia (yellow arrow), 5: Focal accumulation of mononuclear cells around the vascular structure (yellow arrow), 25: Normal histology. Kidney: 0D: Normal histology, PBS: Normal histology, Cis: Tubular necrosis noted in the renal cortex (black arrow), 1.5: Normal histology, 3: Normal histology, 5: Normal histology, 25: Normal histology. Heart: 0D: Normal histology, PBS: Suppurative myocarditis observed, Cis: Tubular necrosis in the renal cortex noted (black arrow), 1.5: Normal histology, 3: Normal histology, 5: Normal histology, 25: Normal histology. Brain: 0D: Normal histology, PBS: Diffuse infiltration of neutrophils (black arrow) in the brain parenchyma, Cis: Normal histology, 1.5: Normal histology, 3: Normal histology, 5: Normal histology, 25: Normal histology. Liver: 0D: Normal histology, PBS: Foci of metastasis (black arrow) in hepatic parenchyma, Cis: Metastatic foci noted (black arrow) in the parenchyma, 1.5: Focal aggregation of inflammatory cells (circle) in the parenchyma, 3: Focal necrosis and accumulation of inflammatory cells (circle), 5: Limited number of neutrophils present in the parenchyma (yellow arrow), 25: Focal necrosis and accumulation of inflammatory cells (circle) (H & E, Scale bar: 50 µm).

In this experiment, mice suffering from lung cancer were observed by a veterinarian throughout the duration of the research study. The veterinarian examined clinical indicators of the mice such as weight, body temperature, behavior, and appearance of feces. From the results shown in Figure 3J, despite mild variations in the weight of the mice, no significant changes in weight were observed during the 15-day study period. Abnormal behavioral patterns in mice were not noted in the veterinary report. Only lethargy was observed. It was also reported that the body temperature of mice administered 25 µg/kg nanodrug was 0.5 to 0.8 degrees higher than that of the other mice. The latter group of mice also reported very dark-colored feces, which can be caused by bleeding in the intestinal tract.

The Nanodrug Alters the Oxidative Stress Levels within the Tumor Microenvironment.

The tumor cells' strategies are to promote an environment in which the redox balance tends towards oxidation by increasing their antioxidant levels. This type of biochemical behavior makes them able to maintain ROS-driven proliferation but avoid ROS levels that would then trigger necrosis, senescence, apoptosis, or ferroptosis.[18] In the present study, SOD levels, which are known to increase in response to increased ROS levels in cells, were quantified as a marker of antioxidant capacity in tumor tissues.[40] On the other hand, the presence of MDA, a byproduct of oxidative stress resulting from the peroxidation of lipids by oxygen radicals, has been evaluated as an indirect marker of oxidative capacity in tumor tissues. The results presented in Figure 5 show an increase in SOD levels of the mice administered cisplatin and nanodrugs compared to those administered PBS alone (Figure 5a). Furthermore, Figure 5b shows reduced MDA levels in mice administered cisplatin and nanodrugs compared to those treated with PBS alone (Figure 5b).

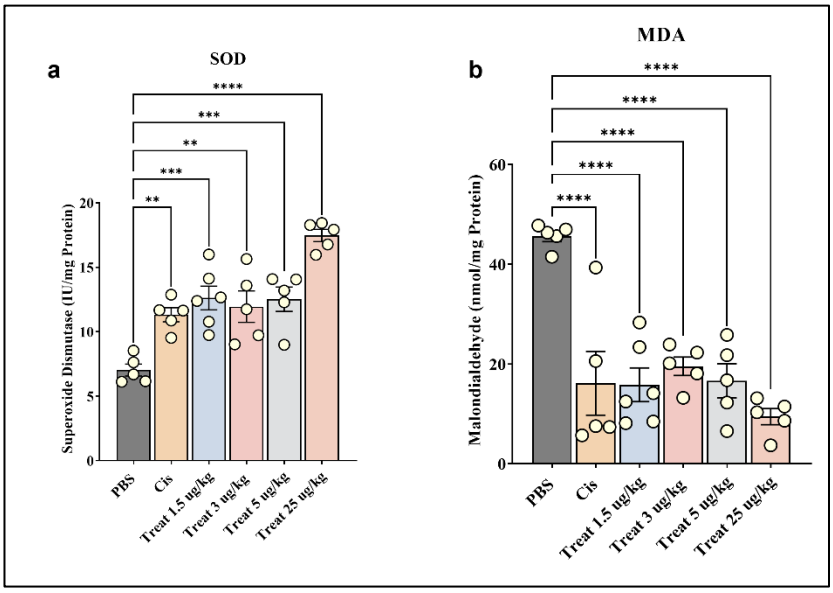

Figure 5. The diagram pertains to the assessment of oxidative stress markers in mice. A. The average superoxide dismutase enzyme factor varied significantly among the mice receiving cisplatin, the nanodrug, and the phosphate-buffered saline (PBS). Statistical analysis using ordinary one-way analysis of variance (ANOVA) revealed a significant difference in the mean values between these groups, with a p = 0.0027. Consequently, post hoc analysis using Tukey's HSD (honestly significant difference) was deemed necessary to further explore these findings. B. The average malondialdehyde (MDA) factor also exhibited significant differences among mice in the cisplatin-, nanodrug-, and PBS-receiving groups. Statistical analysis using one-way ANOVA indicated a significant difference in the mean values between these groups, with a p value of 0.0037. Therefore, post hoc analysis using Tukey's HSD was conducted to provide additional insights into these results, and the levels of MDA and superoxide dismutases (SOD), which are associated with oxidative stress, were assessed in the mice in the 15-day groups. ns: not significant, * p<0.05, ** p<0.01, ***p< 0.001 and ****p< 0.0001.

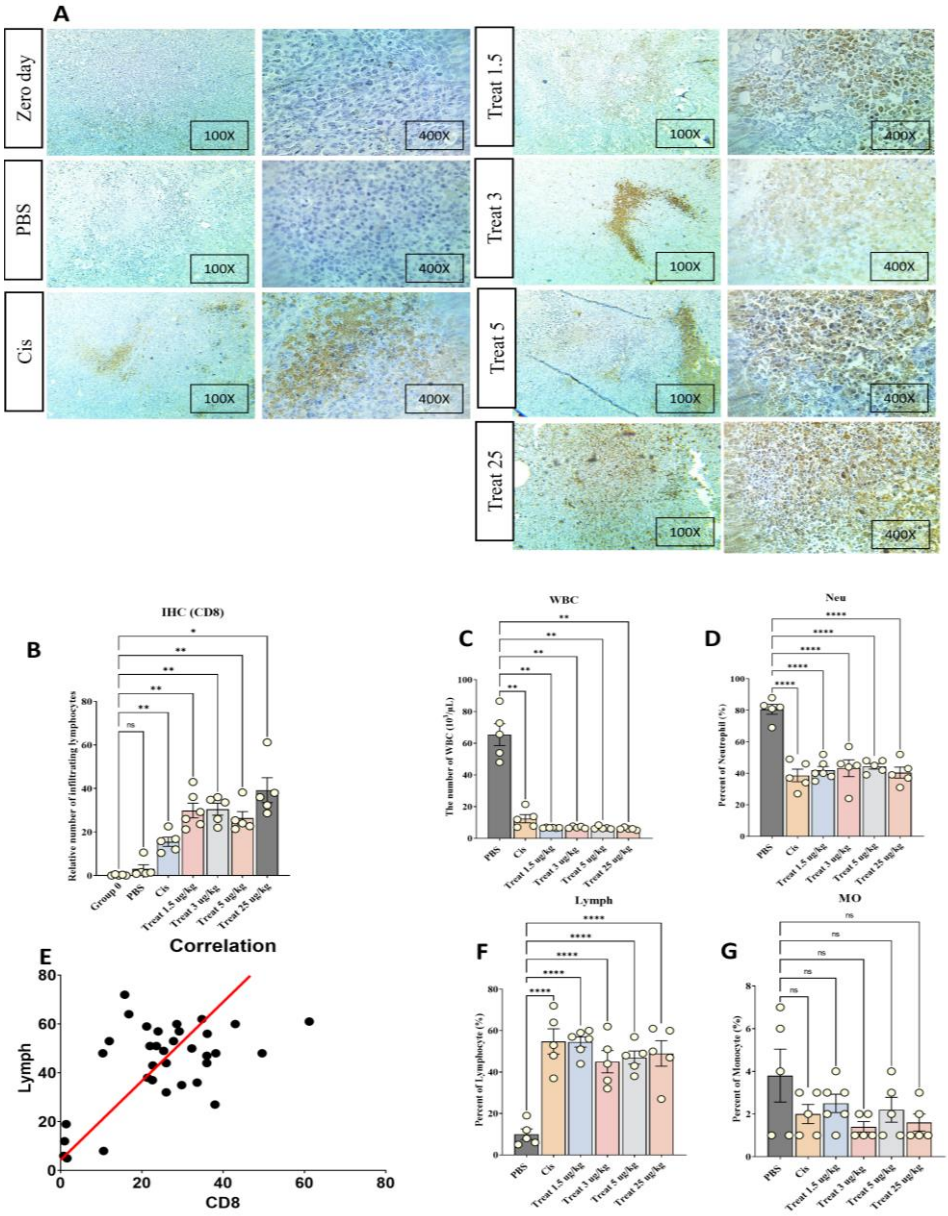

Figure 6. The evaluation of CD8$^+$ cell infiltration into tumor tissue was conducted in this study. A. An immunohistochemical test was performed on tumor tissue samples, and an image of one mouse from the nanodrug, cisplatin, and phosphate-beffered saline (PBS) groups was selected as a representative example. The image was captured at two magnifications, 100 and 400. In the image, cell nuclei were stained blue, while the CD8 marker was stained brown. Notably, the presence of CD8$^+$ cells, indicating lymphocyte infiltration into the tumor tissue, was clearly observed in mice treated with nanodrug. B. Subsequently, the infiltrated cells were counted, and a corresponding statistical analysis was conducted. The normality of the data was assessed using the Shapiro-Wilk test, followed by a one-way analysis of variance (ANOVA) test to compare the groups. The obtained *p* value was 0.0004, indicating a significant difference in the average number of infiltrated cells between the two groups. (C–D, F–G) The results show significant changes in white blood cells (WBC), blood leukocytes, and neutrophils and also no significant changes in monocytes in mice cancer model after nanodrug and cisplatin treatment compared to the control group receiving PBS. The data indicates an increase in CD8$^+$ cell infiltration, the percentage of lymphocytes, and a decrease in the percentage of neutrophils. (E) The findings also demonstrate a positive correlation between changes in lymphocytes in the blood and infiltration of CD8 cells in tissue. ns: not significant, * p<0.05, ** p<0.01, *** p<0.001, and **** p<0.0001.

The Nanodrug Enhances the Infiltration of Lymphocytes into the Tumor Region.

Immune responses play a dual role in human biology. They prevent and promote cancer. Of note, $CD8^+$ T cells have been shown to play a key role in effective immune responses against tumors. An immunohistochemical methodology using CD8 markers was used to evaluate the rate of lymphocyte infiltration in tissue samples from the tumor region. In addition, the changes in blood leukocytes were monitored in the mouse cancer model. The results of this research show that there was a significant increase in the infiltration rate of CD8 cells in the nanodrug and cisplatin-treated groups compared to the first day of research and the PBS-receiving groups, as shown in Figure 6a-b. The changes in leukocytes in the blood were then analyzed. As shown in Figures 6D–F, the percentage of lymphocytes was significantly increased compared to the PBS group, while the percentage of neutrophils was significantly decreased in the nanodrug and cisplatin groups. Figure 6g shows that the percentage of monocytes was similar in all groups and did not differ. The percentages of mice receiving PBS with severe leukocytosis are shown in Figure 6C. Statistically, blood lymphocyte changes were positive for correlates of tissue CD8 cell infiltration, as shown in Figure 6e.

DISCUSSION

Closely examining the nanoparticles we have created for nanomedicine, a lot of potential comes out for their use in healthcare. In the characterization of nanoparticles, there exists valuable insight into how they might perform in medical applications. Their size, as found using Dynamic Light Scattering, is around 458.9 nm in average size, although their sizes do vary somewhat. This variability impacts nanoparticle entry into cells and their effectiveness as treatments. The Zeta Potential Analysis showed that the surface charge of these particles is about −7.8 mV, thus rubbing off positively on their stability in biological scenarios by preventing them from clumping together.[29-32] Field emission scanning electron microscopy (FESEM) gave better resolution on the surface of these nanoparticles. The diversified shape and size, ranging from 17.86 nm to 66.99 nm, may play a considerable role in how well the nanoparticles work in the body.[31,33] X-ray diffraction (XRD) revealed that the nanoparticles were crystalline and amorphous in structure, making them complex and able to affect their performance. Fourier transform infrared (FTIR) spectroscopy showed important chemical groups on the surface of the nanoparticles, like hydroxyl and carbonyl. These groups are important for the chemical interaction of the nanoparticles. Ultraviolet (UV)-visible spectroscopy showed very strong absorption peaks in the UV region, which gives an indication of finely sized particles that could be of potential use for biological fluorescent labeling.[31,33] By using all these different techniques, we've been able to show that these nanoparticles are well-suited for use in nanomedicine. We can control their physical and chemical properties precisely, which means they have the potential to be effective and safe in medical treatments.

The objective of this investigation was to assess the impact of the nanodrug on lung cancer and to analyze some underlying mechanisms of its action. The investigation assessed the influence of nanodrugs on the progression of tumors and their spread to other parts of the body by contrasting their effects with those of PBS and cisplatin. The modifications implemented in this nanodrug were anticipated to exhibit a relatively specific impact on metabolically active cells, while not inducing toxic effects on other normal cells within the body. The results indicated that the nanodrug significantly reduced the size of the tumor compared to the control group treated with PBS, similar to the effect observed in mice treated with cisplatin. Additionally, nearly no occurrences of metastasis were noted in mice subjected to nanodrug, whereas metastasis was observed in mice treated with both PBS and cisplatin. In this investigation, as indicated in Figure 2D, it was established that the novel nanodrug exhibited a notable impact on the survival rate of the experimental mice, in contrast to the mice that were administered the PBS. The findings suggest that the nanodrug shows potential as an effective anti-tumor agent and demonstrates proficiency in impeding the spread of cancer to distant organs.

The hematological, biochemical, and pathological parameters were evaluated for the possible toxicity of the nanodrug. The hematological estimations have shown that the nanodrug did not significantly alter RBC count, hematocrit, hemoglobin, or platelet levels. However, an inclination of the nanodrug dose of 1.5 μg/kg and 3 μg/kg was observed to bring back the RBC levels to normal values, thus showing a potential protective effect against anemia. Kidney biochemical evaluations revealed no significant changes in

parameters of kidney function with the nanodrug compared to cisplatin-treated mice, showing remarkable modulation in creatinine and urea levels indicating malfunctioning of kidneys in such animals. Pathological examinations revealed no evidence of tissue impairment in vital organs due to the nanodrug. In contrast, mice treated with cisplatin showed progressive tissue destruction in their kidneys, as already known for the nephrotoxicity of cisplatin.[41] The mice were well looked after during the experiment, and any adverse effects were monitored by their weight remaining stable and no behavioral changes obvious. However, the 25 μg/kg nanodrug dose-treated group showed slight increases in body temperature and dark-colored feces, hence a slight gastrointestinal effect. In general, it revealed very strong evidence that this new nanodrug can be used as an effective drug against lung cancer. It has been shown to effectively inhibit tumor growth and metastasis and show minimal toxicity, without damage to organs. Further investigations should be conducted to clearly determine the mechanisms of actions of nanodrugs and optimize their therapeutic efficacy. The successful development of these nanodrugs can greatly influence the treatment scenario of lung cancer and offer patients a new effective treatment option.

The activation of ZnO nanoparticles is strongly influenced by oxidative stress factors, which were therefore investigated in this research.[21] ZnO NPs are known to induce ROS production through the release of Zn^{2+} ions and surface reactions that generate superoxide and hydroxyl radicals. These ROS promote oxidative stress in cancer cells, disrupting cellular functions and leading to apoptosis and pyroptosis.[42] It has been shown that activation of zinc oxide nanoparticles and a resulting increase in ROS levels can serve as an effective means of stimulating the immune response.[43] Since $CD8^+$ lymphocytes are key immune cells in the tumor microenvironment, their presence was examined to show whether nanodrug-mediated immune system activation elicited an appropriate immune response. The important aspects of this phenomenon were examined in this study; however, it is important to note that a proper understanding requires further research into other important factors. This would also include detailed mechanisms for programmed cell death and necrosis, the diverse functions of cytotoxic T lymphocytes, and the intricate interactions between multiple inflammatory mediators studying these additional components will give you a more complete picture and allow you to delve deeper into the topic at hand. Of the factors mentioned, the ones mentioned above are the main factors. An overview of the properties of the ZnO nanoparticles is given below before the results are presented.

In 2008, Tian Jia et al demonstrated that ZnO nanoparticles can induce an injury response, resulting in the generation of reactive oxygen radicals and proinflammatory cytokines, along with mitochondrial damage.[44] Actually, such toxicity is directly caused by particle dissolution and subsequent release of the toxic Zn^{2+} ions into cells. It has been shown that $Zn2^+$ accumulation in the lysosomes and caveolae induced the fusion of cell organelles and provoked oxidative cell damage, releasing intracellular Ca^{2+}, mitochondrial depolarization, cytokine release, and cytotoxicity.[44] It is reported that an elevated level of ROS by ZnO NPs causes a variety of adverse effects on the cell, leading to DNA damage,[45] impairment in protein synthesis,[46] and disruption of the mitochondrial membrane.[44] This leads to the release of cytochrome C into the cytosol from the mitochondria membrane rupture and further initiates apoptosis as a downstream effect.[44] In 2023, Kanz et al published an article that focused on protein damage and one of its effects on the immune system. They were able to show that with an elevation of intracellular levels of ROS, the radicals provoke the accumulation of misfolded proteins in the endoplasmic reticulum. The accumulated proteins will then activate a cellular process known as the unfolded protein response (UPR). Within the activated UPR pathways in the stressed cells, the PERK-eIF2α-ATF4 axis plays a significant role that leads to the activation of autophagy.[46] Many studies have shown that after accumulating and being activated in a cell, zinc oxide nanoparticles can activate inflammasomes through the Nrf2-TXNIP-NLRP3 axis. As a result, activation of inflammasomes can initiate the secretion of inflammatory cytokines and provoke cell death through pyroptosis.[47-49]

Previous studies showed that SOD is overexpressed in malignant cells where the levels of ROS are high enough to be damaging to the cell. The nature of this overexpression was to ameliorate the toxic effects of the ROS on the cancerous cells, allowing them to survive.[50] Cancer cells can tolerate ROS up to a threshold level.[43] However, when the level of ROS exceeds this threshold in cancer cells, it can lead to cell death within the tumor tissue.[43] Consequently, elevated levels of SOD along with increased apoptosis and necrosis in the tumor tissue may serve as an indication of heightened cellular

damage induced by ROS. This in turn induces various processes, including apoptosis and autophagy, causing the death of cancer cells. Increased expression of SOD in cisplatin-treated cancer cells has already been reported.[43] Since ZnO NPs induce their action mainly by increasing the ROS levels within the tumor cells, which leads to the disruption of the mitochondrial membrane and an increase in apoptosis and autophagy, it was expected that the modified ZnO Nanoparticles would also elicit a similar kind of response through the elevation of ROS levels. As a consequence, this elevation in ROS would trigger the antioxidant mechanisms of the cancer cells and thus might raise SOD levels, similar to the group treated with cisplatin. The results observed validated this hypothesis. It means that increasing SOD may have dual effects: on one hand, it may reduce the level of ROS and inhibit cell death, thus making tumor cells more resistant to drugs. However, upon failing to prevent cell death, it is released into the TME, where it then reduces oxidative stress and promotes an immune response MDA has been known as an oxidative stress byproduct which increases due to ROS overload in the TME.[51] The results of the study, however, showed that the levels of MDA decreased in the tumorous tissue. From the above findings, it could be concluded that the modified ZnO Nanoparticles are entering metabolically active cells like cancer cells and, on activation, increasing ROS levels that are triggering the antioxidant responses which involves an increase in the SOD level. However, the above increase in SOD seems to lack the ability to inhibit ROS induced by zinc oxide nanoparticles. Consequently, upon the death of cells, SOD will be released into the tumor microenvironment. In that microenvironment, SOD contributes to the diminution of ROS levels, which will consequently decrease related byproducts, such as MDA. Maybe this decrease in oxidative stress within the tumor microenvironment will benefit the activity of immune cells.

Recent evidence has revealed that treatment with different anticancer drugs can initiate or augment $CD8^+$ T cell infiltration within the tumor microenvironment, leading to improved clinical responses for patients with cancer.[52-54] One such drug is pembrolizumab, which is an immune checkpoint blockade (ICB) that targets programmed cell death protein receptor 1 (PD-1) on T-cells. Studies in a preclinical setting have shown that pembrolizumab increases the infiltration of $CD8^+$ T cells within the tumor microenvironment, resulting in increased anti-tumor activity.[55] Another drug, ipilimumab, is an immune checkpoint blockade targeting cytotoxic T lymphocyte-associated antigen 4 (CTLA-4) and has been shown to increase the infiltration of $CD8^+$ T cells within the tumor microenvironment, increasing anti-tumor activity in preclinical studies.[56-58] For that matter, pembrolizumab, and ipilimumab have already been reported as potential molecules to enhance the infiltration of $CD8^+$ T cells into the tumor microenvironment, increasing antitumor activity and thus resulting in better clinical consequences for patients with cancer. Notably, as shown in Figure 6, the percentage of lymphocytes in the blood of mice treated with cisplatin and nanodrugs seemed to have a tremendous increase compared to that group only treated with PBS. This finding suggests that nanodrugs may have the potential to influence the acquired immune system. Compared with the control group that was treated with PBS, this proportion for neutrophils in the blood circulation decreased for mice treated with cisplatin and nanodrugs. Neutrophils are a type of white blood cell that are more significant in their involvement during infections.[59] This was shown to happen in a research study by Zhao Elsi et al through a decrease in the peripheral blood-derived neutrophil-to-lymphocyte ratio (dNLR), which evidences a favorable outcome in increased lymphocyte infiltration into the tumor region and enhanced survival of the mice.[60] Correlation analysis, as seen in Figure 6, of peripheral blood lymphocytes vs. $CD8^+$ cell infiltration, showed an increasing trend for the nanodrug-treated mice, meaning more lymphocyte infiltration into the tumor area. ZnO NPs first increase ROS in tumor cells, leading to oxidative stress, which contributes to cancer cell death. This cytotoxic effect on tumor cells is beneficial for reducing tumor mass and slowing progression. During this initial ROS increase, ZnO NPs give rise to superoxide dismutase (SOD) activity in the TME, which subsequently decreases overall ROS levels. This decrease in ROS in the TME results in a more favorable environment for immune cell function, particularly CTL cells. High levels of ROS are known to inhibit CTL activation and cytotoxicity.[61] By reducing ROS levels in the TME, the ZnO nanoparticles can improve the activation and cytotoxic efficacy of CTL cells infiltrating the tumor tissue. This ROS modulation therefore supports a more effective immune response against tumor cells, facilitates CTL function, and enhances immune-mediated antitumor effects. Lastly,

leukocytosis was observed in mice treated with PBS. High white blood cell count has long been reported in patients with lung carcinoma at the time of report or during the disease process. This can be due to either concurrent infections, bone marrow metastasis, or corticosteroids. However, many cases have been found where lung carcinoma patients develop leukocytosis without the above-mentioned conditions. Such type of leukocytosis, known as tumor-related leukocytosis (TRL), is caused by abnormal production of hematopoietic cytokines with 60% incidence.[62] Over 40 hematopoietic cytokine-producing lung carcinomas have been found so far. Various hematopoietic cytokines have been derived from tumor cells and cloned cell lines established from tumors. As mentioned earlier, the majority of lung carcinomas relate to G-CSF production, while a few are related to the production of GM-CSF and IL-6.[62] The absence of TRL indicates that the mice treated with cisplatin and nanodrugs did not develop this condition, common in severe metastatic conditions as shown in Figure 6. The findings also establish that the nanodrug suppresses the activity of the tumor cells, hence there is no deviation of leukocytes outside the normal range to cause leukocytosis. In summary, the peripheral blood lymphocytes were increased, while the ratio of dNLR was decreased. The proportion of $CD8^+$ lymphocytes within tumor tissue was raised, which means the nanodrug had a positive effect on the immune response against the tumor. Furthermore, no TRL indicates that the nanodrug functions well in maintaining physiological conditions. All these changes present in the blood lead to a more appropriate immune response against tumor cells.

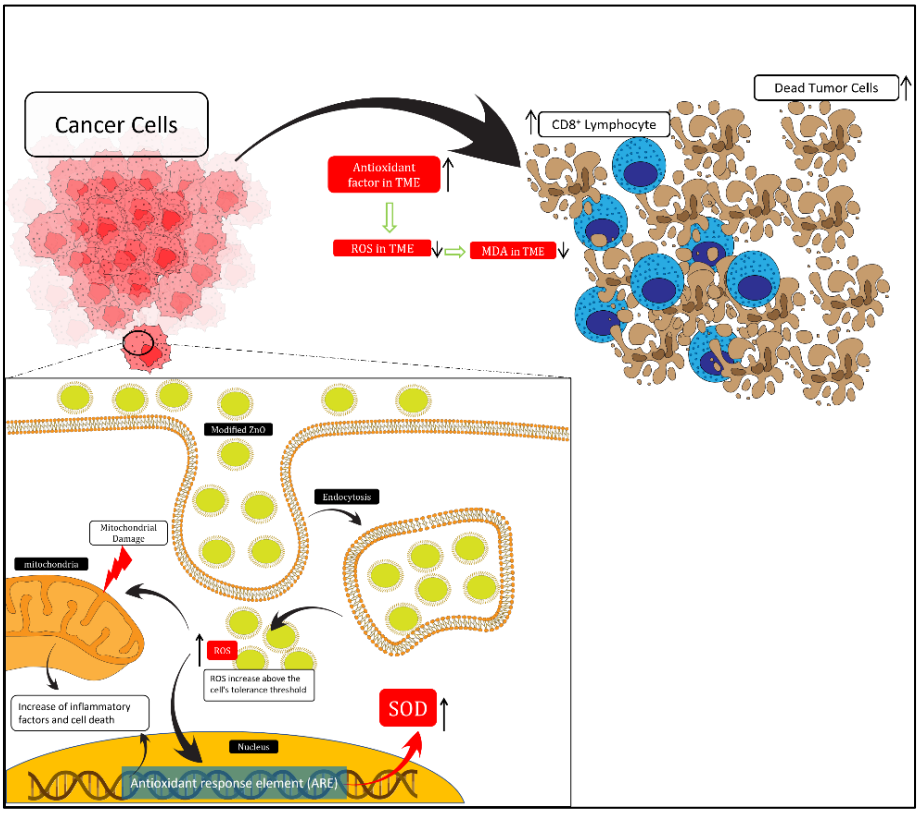

Figure 7. The illustration depicts the hypothesized mechanism through which the nanodrug may exert its pharmacological effects. Zinc oxide-based nanoparticles induce an increase in ROS levels within cancer cells, leading to mitochondrial membrane disruption and promoting apoptosis and autophagy. The nanodrug is expected to have a similar effect by augmenting ROS levels. This increase in ROS activates antioxidant mechanisms within the cancer cells, potentially leading to an increase in SOD levels, similar to the group receiving cisplatin. The findings of the study indicate a decrease in MDA levels within the tumor tissue, suggesting that the nanodrug induces an elevation in ROS levels and triggers antioxidant responses. This decrease in oxidative stress within the tumor microenvironment may be beneficial for the activity of immune cells.

The novel nanodrug was synthesized of nano oxidizing and nano reducing various agents which exhibited remarkable promise as an effective therapeutic strategy for lung cancer. It was characterized by FESEM, XRD, FTIR, DLS, UV-Vis, and Zeta Potential. Nanoparticle components include two categories, amorphous and crystalline structures. The absorption wavelength in UV-Vis was very low, and as a result, the average of all NPs in the nanofluid showed a very small and blue-shift. The surface charge of the NPs in the colloidal nano solution was negative, which could create strong electrostatic attractions with positively charged cancerous tumors in their bio-interface, and as a result, trapped lung cancer cells. Therefore, the penetration power of NPs, contact angles, and wettability alteration in the bio-interface phase with tumor glands became appropriate and they were also able to eliminate the cancer cells through oxidative stress reaction. By modulating the tumor microenvironment through alterations in oxidative stress levels and enhanced lymphocyte infiltration, these strong NPs hold the potential to combat this formidable disease. The promising survival outcomes observed in the mouse model further reinforce the translational potential of this novel nanodrug-based therapy. Further research is warranted to elucidate the underlying mechanisms and optimize the therapeutic efficacy of this promising agent. The successful development of these nanodrugs could change the treatment landscape for lung cancer, providing patients with a modern and effective therapeutic option.

STATEMENT OF ETHICS

The present study has been granted approval by the ethics committee of Shahed University, bearing the code of ethics IR.SHAHED.REC.1401.153.

FUNDING

This research did not receive any grant from funding agencies in the public, commercial, or nonprofit sectors.

CONFLICT OF INTEREST

The authors declare no conflicts of interest.

ACKNOWLEDGMENTS

We express our gratitude to all the individuals who are part of the ARENA laboratory.

DATA AVAILABILITY

Available from the corresponding author upon reasonable request.

AI ASSISTANCE DISCLOSURE

Not applicable.

REFERENCES

1. Aghebati-Maleki A, Dolati S, Ahmadi M, Baghbanzhadeh A, Asadi M, Fotouhi A, et al. Nanoparticles and cancer therapy: Perspectives for application of nanoparticles in the treatment of cancers. J Cell PhysiolP. 2020;235(3):1962-72.
2. Anjum S, Hashim M, Malik SA, Khan M, Lorenzo JM, Abbasi BH, Hano C. Recent advances in zinc oxide nanoparticles (ZnO NPs) for cancer diagnosis, target drug delivery, and treatment. Cancers. 2021;13(18):4570.
3. Jiang J, Pi J, Cai J. The advancing of zinc oxide nanoparticles for biomedical applications. Bioinorg Chem Appl. 2018;2018.
4. Wiesmann N, Tremel W, Brieger J. Zinc oxide nanoparticles for therapeutic purposes in cancer medicine. J Mater Chem B. 2020;8(23):4973-89.
5. Abdolmohammadi MH, Fallahian F, Fakhroueian Z, Kamalian M, Keyhanvar P, M. Harsini F, Shafiekhani A. Application of new ZnO nanoformulation and Ag/Fe/ZnO nanocomposites as water-based nanofluids to consider in vitro cytotoxic effects against MCF-7 breast cancer cells. Artif Cells Nanomed Biotechnol. 2017;45(8):1769-77.
6. Fakhroueian Z, Vahabpour R, Assmar M, Massiha A, Zahedi A, Esmaeilzadeh P, et al. ZnO Q-Dots as a Potent Therapeutic Nanomedicine for in Vitro Cytotoxicity Evaluation of Mouth KB44, Breast MCF7, Colon HT29 and HeLa Cancer Cell Lines, Mouse Ear Swelling Tests in Vivo and Its Side Effects Using the Animal Model. Artif Cells Nanomed Biotechnol. 2018;46(sup2):96-111.
7. Ghaffari S-B, Sarrafzadeh M-H, Fakhroueian Z, Shahriari S, Khorramizadeh MR. Functionalization of ZnO nanoparticles by 3-mercaptopropionic acid for aqueous curcumin delivery: Synthesis, characterization, and anticancer assessment. Mater Sci Eng C Mater Biol Appl. 2017;79:465-72.
8. Lung cancer 26 June 2023 [Available from: https://www.who.int/news-room/fact-sheets/detail/lung-cancer.

9. Rivera MP, Detterbeck F, Mehta AC. Diagnosis of lung cancer: the guidelines. Chest. 2003;123(1):129S-36S.
10. Collins LG, Haines C, Perkel R, Enck RE. Lung cancer: diagnosis and management. Am Family Fhysician. 2007;75(1):56-63.
11. Fennell D, Summers Y, Cadranel J, Benepal T, Christoph D, Lal R, et al. Cisplatin in the modern era: The backbone of first-line chemotherapy for non-small cell lung cancer. Cancer Treat Rev. 2016;44:42-50.
12. Svaton M, Zemanova M, Zemanova P, Kultan J, Fischer O, Skrickova J, et al. Impact of concomitant medication administered at the time of initiation of nivolumab therapy on outcome in non-small cell lung cancer. Anticancer Res. 2020;40(4):2209-17.
13. Hoy H, Lynch T, Beck M. Surgical treatment of lung cancer. Critical Care Nurs Clin. 2019;31(3):303-13.
14. Inoue M, Sawabata N, Okumura M. Surgical intervention for small-cell lung cancer: what is the surgical role? General thoracic and cardiovascular surgery. 2012;60:401-5.
15. Lackey A, Donington JS, editors. Surgical management of lung cancer. Semin Intervent Radiol. 2013;30(2):133-40.
16. Carbone DP, Gandara DR, Antonia SJ, Zielinski C, Paz-Ares L. Non–small-cell lung cancer: role of the immune system and potential for immunotherapy. J Thoracic Oncol. 2015;10(7):974-84.
17. Caliri AW, Tommasi S, Besaratinia A. Relationships among smoking, oxidative stress, inflammation, macromolecular damage, and cancer. Mut Res Rev Mut Res. 2021;787:108365.
18. Hayes JD, Dinkova-Kostova AT, Tew KD. Oxidative stress in cancer. Cancer cell. 2020;38(2):167-97.
19. Reuter S, Gupta SC, Chaturvedi MM, Aggarwal BB. Oxidative stress, inflammation, and cancer: how are they linked? Free Radic Biol Med. 2010;49(11):1603-16.
20. Prado-Garcia H, Romero-Garcia S, Aguilar-Cazares D, Meneses-Flores M, Lopez-Gonzalez JS. Tumor-induced CD8+ T-cell dysfunction in lung cancer patients. Clin Develop Immunol. 2012;2012.
21. Bisht G, Rayamajhi S. ZnO nanoparticles: a promising anticancer agent. Nanobiomedicine. 2016;3:9.
22. Horie M, Tabei Y. Role of oxidative stress in nanoparticles toxicity. Free Radic Res. 2021;55(4):331-42.
23. Pandurangan M, Veerappan M, Kim DH. Cytotoxicity of zinc oxide nanoparticles on antioxidant enzyme activities and mRNA expression in the cocultured C2C12 and 3T3-L1 cells. Appl Biochem Biotechnol. 2015;175:1270-80.
24. Hira I, Kumar A, Kumari R, Saini AK, Saini RV. Pectin-guar gum-zinc oxide nanocomposite enhances human lymphocytes cytotoxicity towards lung and breast carcinomas. Mater Sci Eng C Mater Biol Appl. 2018;90:494-503.
25. Fakhroueian Z. Synthesis and in vitro Evaluation of A Green Nanomedicine for the Treatment of Pa-tients with COVID-19 Virus and Lung and Breast Cancers. J Nanotech Smart Mater. 2022;8:1-21.
26. Aston WJ, Hope DE, Nowak AK, Robinson BW, Lake RA, Lesterhuis WJ. A systematic investigation of the maximum tolerated dose of cytotoxic chemotherapy with and without supportive care in mice. BMC cancer. 2017;17(1):1-10.
27. Perše M. Cisplatin mouse models: Treatment, toxicity and translatability. Biomedicines. 2021;9(10):1406.
28. Boland J, Atkinson K, Britton K, Darveniza P, Johnson S, Biggs J. Tissue distribution and toxicity of cyclosporin A in the mouse. Pathology. 1984;16(2):117-23.
29. Hashemi S, Asrar Z, Pourseyedi S, Nadernejad N. Green synthesis of ZnO nanoparticles by Olive (Olea europaea). IET nanobiotechnology. 2016;10(6):400-4.
30. Nalwa K, Thakur A, Sharma N. Synthesis of ZnO nanoparticles and its application in adsorption. Advanced Materials Proceedings. 2017;2(11):697-703.
31. Fakhroueian Z, Vahabpour R, Assmar M, Massiha A, Zahedi A, Esmaeilzadeh P, et al. ZnO Q-dots as a potent therapeutic nanomedicine for in vitro cytotoxicity evaluation of mouth KB44, breast MCF7, colon HT29 and HeLa cancer cell lines, mouse ear swelling tests in vivo and its side effects using the animal model. Artif Cells Nanomed Biotechnol. 2018;46(sup2):96-111.
32. Suganthi K, Rajan K. Temperature induced changes in ZnO–water nanofluid: zeta potential, size distribution and viscosity profiles. Int J Heat Mass Transfer. 2012;55(25-26):7969-80.
33. Fakhroueian Z, Massiha A, Esmaeilzadeh P, Assmar M, Zahedi A, Esmaeilzadeh P, et al. In vivo animal model evaluation of a powerful oral nanomedicine for treating breast cancer in BALB/c mice using 4T1 cell lines without chemotherapy. Adv Nanoparticles. 2022;11(03):73-109.
34. Aftab S, Shah A, Nadhman A, Kurbanoglu S, Ozkan SA, Dionysiou DD, et al. Nanomedicine: An effective tool in cancer therapy. Int J Pharmaceutics. 2018;540(1-2):132-49.
35. Liang C, Xu L, Song G, Liu Z. Emerging nanomedicine approaches fighting tumor metastasis: animal models, metastasis-targeted drug delivery, phototherapy, and immunotherapy. Chem Society Rev. 2016;45(22):6250-69.
36. Gupta R, Polaka S, Rajpoot K, Tekade M, Sharma MC, Tekade RK. Importance of toxicity testing in drug

discovery and research. Pharmacokinetics and toxicokinetic considerations: Elsevier; 2022. p. 117-44.
37. Preham O, Pinho FA, Pinto AI, Rani GF, Brown N, Hitchcock IS, et al. CD4+ T cells alter the stromal microenvironment and repress medullary erythropoiesis in murine visceral leishmaniasis. Front Immunol. 2018;9:2958.
38. Lyman JL. Blood urea nitrogen and creatinine. Emerg Med Clin North Am. 1986;4(2):223-33.
39. Lala V, Zubair M, Minter DA. Liver function tests. StatPearls [internet]: StatPearls Publishing; 2022.
40. Aboelella NS, Brandle C, Kim T, Ding Z-C, Zhou G. Oxidative stress in the tumor microenvironment and its relevance to cancer immunotherapy. Cancers. 2021;13(5):986.
41. Peres LAB, Cunha Júnior ADd. Acute nephrotoxicity of cisplatin: molecular mechanisms. Brazilian J Nephrol. 2013;35:332-40.
42. Biswas A, Kar U, Jana NR. Cytotoxicity of ZnO nanoparticles under dark conditions via oxygen vacancy dependent reactive oxygen species generation. Phys Chem Chem Phys. 2022;24(22):13965-75.
43. Rasmussen JW, Martinez E, Louka P, Wingett DG. Zinc oxide nanoparticles for selective destruction of tumor cells and potential for drug delivery applications. Expert Opin Drug Deliv. 2010;7(9):1063-77.
44. Xia T, Kovochich M, Liong M, Madler L, Gilbert B, Shi H, et al. Comparison of the mechanism of toxicity of zinc oxide and cerium oxide nanoparticles based on dissolution and oxidative stress properties. ACS nano. 2008;2(10):2121-34.
45. Penning TM. Genotoxicity of ortho-quinones: reactive oxygen species versus covalent modification. Toxico Res. 2017;6(6):740-54.
46. Di Conza G, Ho P-C, Cubillos-Ruiz JR, Huang SC-C. Control of immune cell function by the unfolded protein response. Nat Rev Immunol. 2023:1-17.
47. Zhang L, Chu W, Zheng L, Li J, Ren Y, Xue L, et al. Zinc oxide nanoparticles from Cyperus rotundus attenuates diabetic retinopathy by inhibiting NLRP3 inflammasome activation in STZ-induced diabetic rats. J Biochem Mol Toxicol. 2020;34(12):e22583.
48. Liang X, Zhang D, Liu W, Yan Y, Zhou F, Wu W, Yan Z. Reactive oxygen species trigger NF-κB-mediated NLRP3 inflammasome activation induced by zinc oxide nanoparticles in A549 cells. Toxicol Indust Health. 2017;33(10):737-45.
49. Abd El-Khalik SR, Nasif E, Arakeep HM, Rabah H. The prospective ameliorative role of zinc oxide nanoparticles in STZ-induced diabetic nephropathy in rats: Mechanistic targeting of autophagy and regulating Nrf2/TXNIP/NLRP3 inflammasome signaling. Bioll Trace Element Res. 2022:1-11.
50. Morelli AP, Tortelli Jr TC, Pavan ICB, Silva FR, Granato DC, Peruca GF, et al. Metformin impairs cisplatin resistance effects in A549 lung cancer cells through mTOR signaling and other metabolic pathways. Intl J Oncol. 2021;58(6):1-15.
51. Singh Z, Karthigesu IP, Singh P, Rupinder K. Use of malondialdehyde as a biomarker for assessing oxidative stress in different disease pathologies: a review. Iran J Public Health. 2014;43(Supple 3):7-16.
52. Mahmoud SM, Paish EC, Powe DG, Macmillan RD, Grainge MJ, Lee AH, et al. Tumor-infiltrating CD8+ lymphocytes predict clinical outcome in breast cancer. J Clin Oncol. 2011;29(15):1949-55.
53. Li F, Li C, Cai X, Xie Z, Zhou L, Cheng B, et al. The association between CD8+ tumor-infiltrating lymphocytes and the clinical outcome of cancer immunotherapy: A systematic review and meta-analysis. EClinical Medicine. 2021;41.
54. Deschoolmeester V, Baay M, Van Marck E, Weyler J, Vermeulen P, Lardon F, Vermorken JB. Tumor infiltrating lymphocytes: an intriguing player in the survival of colorectal cancer patients. BMC Immunol. 2010;11(1):1-12.
55. Sakatani T, Kita Y, Fujimoto M, Sano T, Hamada A, Nakamura K, et al. IFN-gamma expression in the tumor microenvironment and CD8-positive tumor-infiltrating lymphocytes as prognostic markers in urothelial cancer patients receiving pembrolizumab. Cancers. 2022;14(2):263.
56. Perez BA, Kim S, Wang M, Karimi AM, Powell C, Li J, et al. Prospective single-arm phase 1 and 2 study: ipilimumab and nivolumab with thoracic radiation therapy after platinum chemotherapy in extensive-stage small cell lung cancer. Int J Radiat Oncol Biol Phys. 2021;109(2):425-35.
57. Madonna G, Ballesteros-Merino C, Feng Z, Bifulco C, Capone M, Giannarelli D, et al. PD-L1 expression with immune-infiltrate evaluation and outcome prediction in melanoma patients treated with ipilimumab. Oncoimmunology. 2018;7(12):e1405206.
58. Arriola E, Wheater M, Lopez MA, Thomas G, Ottensmeier C. Evaluation of immune infiltration in the colonic mucosa of patients with ipilimumab-related colitis. Oncoimmunology. 2016;5(9):e1209615.
59. Di Carlo E, Forni G, Lollini P, Colombo MP, Modesti A, Musiani P. The intriguing role of polymorphonuclear

neutrophils in antitumor reactions. Blood. 2001;97(2):339-45.

60. Alessi JV, Ricciuti B, Alden SL, Bertram AA, Lin JJ, Sakhi M, et al. Low peripheral blood derived neutrophil-to-lymphocyte ratio (dNLR) is associated with increased tumor T-cell infiltration and favorable outcomes to first-line pembrolizumab in non-small cell lung cancer. J Immunotherapy Cancer. 2021;9(11).
61. Belikov AV, Schraven B, Simeoni L. T cells and reactive oxygen species. J Biomed Sci. 2015;22:1-11.
62. Kasuga I, Makino S, Kiyokawa H, Katoh H, Ebihara Y, Ohyashiki K. Tumor-related leukocytosis is linked with poor prognosis in patients with lung carcinoma. Cancer. 2001;92(9):2399-405.